Journal of Power Sources 188 (2009) 411–420

Contents lists available at ScienceDirect

Journal of Power Sources

journal homepage: www.elsevier.com/locate/jpowsour

Hydrogen generation by hydrolysis of $NaBH_4$ with efficient Co–P–B catalyst: A kinetic study

N. Patel*, R. Fernandes, A. Miotello

Dipartimento di Fisica, Università degli Studi di Trento, Via Sommarive 14, I-38100 Povo (Trento), Italy

ARTICLE INFO

Article history:
Received 11 September 2008
Received in revised form
18 November 2008
Accepted 29 November 2008
Available online 6 December 2008

Keywords:
H_2 generation
Hydrolysis
Sodium borohydride
Co–P–B catalyst
Kinetic study

ABSTRACT

Amorphous catalyst alloy powders in form of Co–P, Co–B, and Co–P–B have been synthesized by chemical reduction of cobalt salt at room temperature for catalytic hydrolysis of $NaBH_4$. Co–P–B amorphous powder showed higher efficiency as a catalyst for hydrogen production as compared to Co–B and Co–P. The enhanced activity obtained with Co–P–B (B/P molar ratio = 2.5) powder catalyst can be attributed to: large active surface area, amorphous short range structure, and synergic effects caused by B and P atoms in the catalyst. The roles of metalloids (B and P) in Co–P–B catalyst have been investigated by regulating the B/P molar ratio in the starting material. Heat-treatment at 773 K in Ar atmosphere causes the decrease in hydrogen generation rate due to partial Co crystallization in Co–P–B powder. Kinetic studies on the hydrolysis reaction of $NaBH_4$ with Co–P–B catalyst reveal that the concentrations of both NaOH and catalyst have positive effects on hydrogen generation rate. Zero order reaction kinetics is observed with respect to $NaBH_4$ concentration with high hydride/catalyst molar ratio while first order reaction kinetics is observed at low hydride/catalyst molar ratio. Synergetic effects of B and P atoms in Co–P–B catalyst lowers the activation energy (32 kJ mol^{-1}) for hydrolysis of $NaBH_4$. The stability, reusability, and durability of Co–P–B catalyst have also been investigated and reported in this work. It has been found that by using B/P molar ratio of 2.5 in Co–P–B catalyst, highest H_2 generation rate of about ~4000 ml min^{-1} g^{-1} can be achieved. This can generate 720 W for Proton Exchange Membrane Fuel Cells (0.7 V): which is necessary for portable devices.

1. Introduction

In the near future, hydrogen has been identified as an attractive candidate for energy carrier by using it as a fuel in proton exchange membrane fuel cell (PEMFC). On industrial level, H_2 is mostly produced by steam reforming of natural gas; but the final product contains carbon contamination (CO_2 and CO). The carbon contamination reduces the performance of PEMFC by catalyst poisoning [1]. For this reason, chemical hydrides are potential candidate materials for pure hydrogen supply to fuel cells at room temperature [2]. Among them, aqueous sodium borohydride ($NaBH_4$) seems to be an ideal hydrogen source because it is stable, non-flammable, non-toxic in nature, and with hydrogen storing capability of 10.8 wt%. [3]. The reaction product (borax), obtained after de-hydrogenation of $NaBH_4$, is environmentally clean and can be recycled to generate the reactant [4]. Hydrogen is generated by water based hydrolysis reaction of $NaBH_4$ with the important advantage of producing half of the hydrogen from the water solvent [5]. These distinct advantages of hydrogen generation from $NaBH_4$ hydrolysis make it a promising on-board hydrogen generation method for portable PEM fuel cells.

The efficiency of hydrogen production can be significantly enhanced by use of catalyst during the hydrolysis reaction. Many organic and inorganic acids are able to enhance the hydrolysis reaction rate, however the reaction usually becomes uncontrollable [6]. On the other hand, solid state catalysts such as precious metals (generally functionalized with support) or transition metals and their salts are found to be very efficient in accelerating the hydrolysis reaction in a controllable manner. Noble catalysts like Pt [7] and Pd [8] supported on carbon, PtRu supported on metal oxide [9], Ru supported on anion-exchange resin [10], Ru nanoclusters [11], and Ru-promoted sulphated zirconia [12] have been utilized in the past to enhance the hydrogen production rate. However, such catalysts seem to be not viable for the industrial application considering their cost and availability. Transition metals such as fluorinated Mg based alloy [13], Raney Ni and Co, nickel and cobalt borides [14–16], and even metal salts are generally used to accelerate the hydrolysis reaction of $NaBH_4$. Co and Ni borides are considered as good candidates for catalyzed hydrolysis reaction of $NaBH_4$ owing to their good catalytic activity and low cost. These catalyst materials can be effortlessly synthesized by a simple chemical reduction method in

* Corresponding author. Tel.: +39 3407988590; fax: +39 0461881696.
E-mail address: patel@science.unitn.it (N. Patel).

0378-7753/$ – see front matter © 2008 Elsevier B.V. All rights reserved.
doi:10.1016/j.jpowsour.2008.11.121

which transition metal ions are brought to the metallic state by a reducing agent [15]. In our previous work, Co–B catalysts developed in the form of nano-particle assembled films by using pulsed laser deposition technique, showed a performance similar to that of the noble metals [16,17].

However, these non-noble metals (Co and Ni) show superior catalytic activity only when used in their boride forms because boron is able to protect the active metal sites (Co or Ni) against oxidation by electron transfer [18]. Metalloid atoms, like boron or phosphorous, have been used with Co (Co–B, Co–P) or Ni (Ni–B, Ni–P) to bring variation in the electronic states of the active metals for superior catalytic activity [19,20]. This shows that metalloids like boron or phosphorous affect the surface properties of catalysts and, hence, their catalytic properties. In the past, it was also reported that the catalytic activity of Co–B is enhanced by inclusion of P in the catalyst. Better selectivity and activity were obtained for the hydrogenation of maltose with Co–P–B catalyst powder, as compared to Co–B and Co–P [21]. A similar effect was reported for Ni in reference [22] where the authors showed that by just regulating the P/B molar ratios, the ultrafine Ni–P–B amorphous alloy catalyst could be made more efficient for various liquid phase hydrogenation reaction than Ni–B or Ni–P.

It is essential to know the role of reactant concentrations in hydrolysis reaction and catalyst behavior in different conditions before designing the reactor for the on-board application. This can be achieved by obtaining the kinetic rate expression for catalytic hydrolysis reaction of alkaline $NaBH_4$ solution. Kreevoy et al. [23] in 1970s broadly investigated the kinetics of acid catalyzed hydrolysis reaction of $NaBH_4$, but very few studies have been reported for the kinetics on metal catalyzed hydrolysis reaction. A new insight into the kinetics of Pd/C catalyzed hydrolysis reaction of $NaBH_4$ using ^{11}B NMR measurements has been recently reported by Guella et al. [8]. In other recent reports, Zhang et al. [24] and Demirci et al. [25] have successfully provided the kinetic rate expression for the $NaBH_4$ hydrolysis reaction on Ni and Ru catalysts respectively.

In the present work, we have synthesized Co–P–B catalyst powders with different B/P molar ratio by chemical reduction method. Superior catalytic behavior has been found to be exhibited by Co–P–B powder as compared to Co–B and Co–P powders, which was inferred from the XPS and morphological studies. The core electron binding energies of Co, P, and B obtained from XPS measurements helped us to infer on the electronic states of Co–P–B, Co–B, and Co–P and to suggest their roles in $NaBH_4$ hydrolysis process. Kinetic rate expression has been obtained for the hydrolysis of alkaline $NaBH_4$ solution over Co–P–B catalyst powder by varying the concentration of reactants ($NaBH_4$, NaOH, and Co–P–B catalyst) and solution temperature. In another set of experiments, reusability and stability of the Co–P–B catalyst powder have been studied and reported.

2. Experimental

2.1. Catalyst preparation

Co–P–B powder catalyst was synthesized by the chemical reduction method. Sodium borohydride ($NaBH_4$), used as a reducing agent, was added into an aqueous solution containing cobalt salt ($CoCl_2$) and sodium hypophosphite (NaH_2PO_2) under vigorous stirring. The black powder separated from the solution during reaction course was filtered and then extensively washed with distilled water and ethanol before drying at around 323 K under continuous N_2 flow. In order to have the complete reduction of cobalt salt, the molar ratio of (P + B)/Co was kept at about 4. The molar concentrations of $NaBH_4$ and NaH_2PO_2 were adjusted to have different molar ratio of B/P in the Co–P–B powder. For comparison, Co–B and Co–P powders were also synthesized. The Co–B powder was prepared by similar method as Co–P–B, but in absence of NaH_2PO_2. The Co–P powder was prepared as reported elsewhere [22] by heating the aqueous solution of $CoCl_2$ and NaH_2PO_2 at 343 K under vigorous stirring. The pH value (equal to 11) was controlled by using NaOH solution. The Co–P–B catalyst powder was annealed at different temperatures up to 773 K for 2 h in Ar atmosphere to study the effect of the lattice structural variation on the catalytic activity.

2.2. Catalyst characterization

The surface morphology of all catalyst powders was studied by scanning electron microscope (SEM-FEG, JSM 7001F, JEOL) equipped with energy-dispersive spectroscopy analysis (EDS, INCA PentaFET-x3) to determine the composition of the samples. Structural characterization of the catalyst powders was done by conventional X-ray diffraction (XRD) using the Cu Kα radiation ($\lambda = 1.5414$ Å) in Bragg–Brentano (θ–2θ) configuration. Studies of surface electronic states and composition of the catalysts were carried out using X-ray photoelectron spectroscopy (XPS). X-ray photoelectron spectra were acquired using a SCIENTA ESCA200 instrument equipped with a monochromatic Al Kα (1486.6 eV) X-ray source and a hemispherical analyzer. No electrical charge compensation was done to perform the analysis.

2.3. Hydrogen generation measurement

For catalytic activity measurements, an alkaline-stabilized solution of sodium borohydride (pH 13, 0.025 ± 0.001 M) (Rohm and Haas), was prepared by addition of NaOH. The titre of reagent was independently measured through iodometric method [26]. The generated hydrogen quantity was measured through a gas volumetric method in an appropriate reaction chamber with thermostatic bath, wherein the temperature was kept constant within accuracy ±0.1 K. The chamber was equipped with pressure sensor, stirrer system, catalyst insertion device, and also coupled with an electronic precision balance to accurately measure the weight of water displaced by the hydrogen produced during the reaction course. A detailed description of the measurement apparatus is reported in reference [27]. In all the runs, the catalyst was placed on the appropriate device inside the reaction chamber and the system was sealed. Catalyst powder was added to 200 ml of the above solution, at 298 K, under continuous stirring. In order to make comparison, the stoichiometric hydrogen production yield (%) versus time was plotted instead of the hydrogen volume (ml) versus time.

2.4. Kinetic studies

Rate equation was obtained by kinetic studies of $NaBH_4$ hydrolysis on Co–P–B catalyst by varying different process parameters such as solution temperature, starting concentration of catalyst, NaOH and $NaBH_4$. Fresh Co–P–B catalyst was used each time to acquire the kinetic data. H_2 generation rate was measured at different solution temperatures of 298, 303, 308, and 313 K, in order to determine the activation energy involved in the catalytic hydrolysis reaction by Co–P–B powder. Several concentrations of NaOH (0.25–2.50 M), $NaBH_4$ (0.005–0.250 M), and catalyst (10–30 mg) were utilized for the activity measurements in which one parameter was varied while the other parameters were kept constant. In another set of experiment, Co–P–B powder of 200 mg was prepared and kept exposed to air at ambient condition in order to check the stability against deactivation of the catalyst. The catalytic activity for this Co–P–B powder was measured at an interval of about 10–12 days. In another set of experiment, the catalyst powder was recovered after the catalytic activity measurement and re-tested. Before testing, the recovered powder was washed and dried with the same

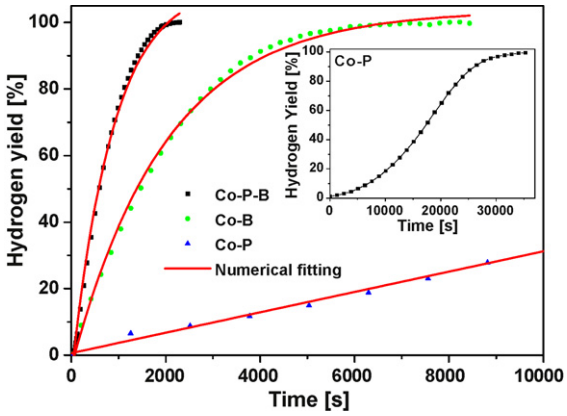

Fig. 1. Hydrogen generation yield as a function of reaction time obtained by hydrolysis of alkaline $NaBH_4$ (0.025 M) solution with Co–B, Co–P, and Co–P–B (B/P molar ratio = 2.5) catalyst powders. Inset shows the extended plot of hydrogen generation yield as function of time for Co–P catalyst.

Table 1
Maximum hydrogen generation rate obtained from the hydrolysis of alkaline $NaBH_4$ (0.025 M) solution by the catalyst powders.

Catalyst powder (15 mg)	Maximum H_2 generation rate, R_{max} (ml min^{-1} g^{-1} catalyst)
Co–B	~850
Co–P	~100
Co–P–B	~2120

procedure mentioned above. This step was repeated several times to establish the reusability of the Co–P–B powder.

3. Results and discussion

3.1. Catalyst activity measurement

Fig. 1 presents the hydrogen generation yield as a function of time obtained from the hydrolysis of alkaline $NaBH_4$ (0.025 M) solution with Co–P, Co–B, and Co–P–B catalyst powders at 298 K. The B/P molar ratio of 2.5 was used in Co–P–B catalyst. The expected total amount of H_2 was measured, irrespective of the type of catalyst used. The inset in Fig. 1 shows the extended plot of the hydrogen generation yield as function of time for Co–P catalyst. The Co–P–B catalyst shows much higher catalytic activity as compared to the same amount (15 mg) of Co–B and Co–P powder. A numerical procedure, described elsewhere [17], was utilized to obtain the maximum values of hydrogen generation rate (R_{max}): these values are summarized in Table 1. The Co–P catalyst powder yields negligible R_{max} as compared to that by Co–B and Co–P–B catalyst powders. On the contrary, the Co–P–B catalyst yields the highest R_{max} which is about 2.5 times higher than that obtained for Co–B catalyst.

3.2. Catalyst characterization

In Fig. 2 we present SEM images of Co–B, Co–P, and Co–P–B (molar ratio B/P = 2.5) powders. The SEM images of Co–B and Co–P–B powders show particle like morphology with average particle size in the range between 30–40 nm. In the cases of Co–B and Co–P–B catalyst preparations, an efficient reducing agent in the form of $NaBH_4$ was utilized which is able to cause the rapid reduction of Co ions and thus it does not permit the particles to grow above a few nanometers. This kind of morphology is helpful in enhancing the active surface area of catalyst. On the contrary, crystallite structure (Fig. 2b) with bigger irregular particles is clearly visible in the case of Co–P catalyst. The reduction of Co ions proceeds gradually in presence of NaH_2PO_2 due to its lower strength as a reducing agent, as compared to that of $NaBH_4$, allowing the growth of large particles in Co–P catalyst. Thus, small surface area achieved in Co–P catalyst might be one of the reasons for the low efficiency of Co–P powder for H_2 generation.

XRD patterns (figure not shown) of Co–B, Co–P, and Co–P–B (with molar ratio B/P = 2.5) powders show a single broad peak at around $2\theta = 45^\circ$ attributed to the amorphous state of cobalt–metalloid alloy [28]. This indicates that all the catalyst powders produced by chemical reduction method are amorphous. It may be inferred that a short-range ordered and long-range disordered structure might be helpful for the catalytic activity [29].

To understand the enhanced efficiency of Co–P–B (with molar ratio B/P = 2.5) catalyst and low efficiency of Co–P catalyst, it is necessary to gain insight into the surface electronic interaction between the elemental atoms in the compound. Thus, XPS spectra of Co–B, Co–P, and Co–P–B (with molar ratio B/P = 2.5) catalyst powders were acquired and are shown in Fig. 3. For Co–B and Co–P–B catalyst powders, two peaks appear corresponding to the $Co_{2p3/2}$ level at the binding energies of 778.4 and 781.6 eV, indicating that Co metal exists in both elemental and oxidized states respectively. On the contrary, only one peak appears corresponding to the $Co_{2p3/2}$ level for Co–P catalyst, at the binding energy of 781.6 eV, signifying that the element cobalt is present in completely oxidized state. The peak due to oxidized cobalt is mainly present in form of +2 state attributed to $Co(OH)_2$, which would have been formed during the catalyst preparation reaction between the reducing agent and the metal salt in aqueous medium [30,31]. The amount of $Co(OH)_2$ is minimum in Co–P–B catalyst as compared to Co–B and Co–P. Two XPS peaks with binding energy (BE) of 188.2 and 192.1 eV are also observed corresponding to the B 1s level in Co–B and Co–P–B, which are assigned to elemental and oxidized boron respectively [30]. By comparing the BE of pure boron (187.1 eV) [32] with that of boron in the catalyst, one observe a positive shift of 1.1 eV. This shift indicates an electron transfer from alloying B to vacant d-orbital of metallic Co which makes the boron atom electron deficient and the cobalt atom enriched with electrons in the catalyst powders. In the X-ray photoelectron spectra corresponding to the P 2p level, one observes signature of two kinds of phosphorous species in Co–P–B catalyst producing peaks with binding energy of 130 eV and 133.3 eV. The

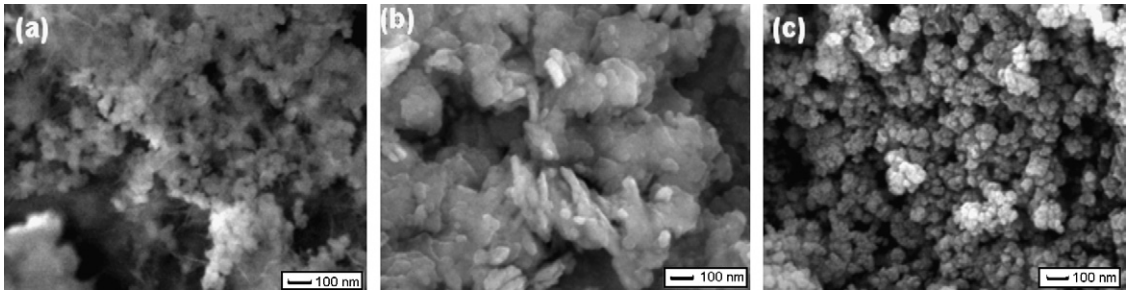

Fig. 2. SEM micrographs of (a) Co–B, (b) Co–P, and (c) Co–P–B (B/P molar ratio = 2.5) catalyst powders.

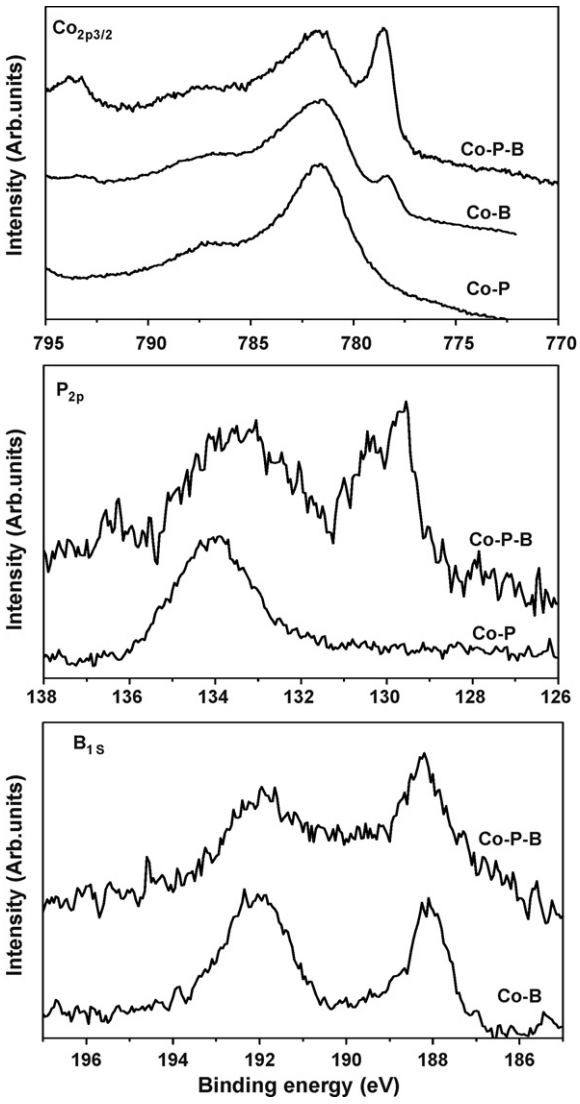

Fig. 3. X-ray photoelectron spectra of $Co_{2p3/2}$, P_{2p}, and B_{1s} level for Co–B, Co–P, and Co–P–B (B/P molar ratio = 2.5) catalyst powders.

lower BE is attributed to the metallic phosphorous while the higher BE is assigned to the oxidized phosphorous. No significant shift in BE of metallic phosphorous was observed with respect to the elemental one, indicating that the electron transfer between Co and P in Co–P–B could be neglected. However in Co–P catalyst powder only BE peak due to oxidized phosphorous is seen.

The above XPS results are now considered to understand the differences observed in catalytic activity with different catalyst powders. In the case of Co–B and Co–P–B catalyst, boron interacts with cobalt by transferring electron from alloying B to vacant d-orbital of metallic Co which makes boron electron-deficient and Co electron-enriched. Looking at the mechanism proposed for metal catalyzed hydrolysis of $NaBH_4$ in our previous work (see Guella et al. [8]), electron-enriched metal active sites will be able to facilitate the catalysis reaction by providing the electron required by the hydrogen atom to leave the metal site in hydridic form (H^-) which then could react with the water molecule to produce H_2 and OH^- ion. This means that the higher electron density on active metal site is an important aspect for the enhancement of the catalytic activity of catalyst powder for hydrolysis of $NaBH_4$, as in the present case of Co–B and Co–P–B catalysts. To this purpose, note that the XPS result clearly shows that there is no electronic interaction between Co and P atoms in Co–P catalyst. The XPS analysis of Co–P powder prepared in a similar manner, as reported by H. Li et al. [21], showed no electronic transfer between Co and P. However, in the literature, many contradictory results are reported for the Ni–P powder: observation of some authors [33,34] are similar to our Co–P powder while others [22,35] showed that there is an electron transfer from Ni to P atoms making the former element electron deficient. Electron transfer also plays an important role in the oxide formation on the surface of the active metal sites. In Co–B and Co–P–B catalysts, electron-enriched metal active sites repel the adsorption of oxygen atoms from the ambient atmosphere, while they are strongly adsorbed by the electron-deficient B. In other words, alloying B effectively protects metals from oxidation in ambient condition [36,37]. Due to the lack of electronic interaction between metal and metalloid in Co–P catalyst, P is unable to protect Co from oxidation. This is clearly evidenced by the fact that Co on the surface is in form of completely oxidized state in our Co–P catalyst powder as observed in the XPS spectra. Hence it seems that the lack of electronic interaction between Co and P atoms might be the main reason for the less active nature of Co–P as catalyst in hydrolysis of $NaBH_4$ as compared to Co–B and Co–P–B catalysts.

The surface atomic composition, calculated from XPS spectra, shows that the amount of the surface Co sites is maximum for Co–P (~77 at.%) and minimum for Co–B (~60 at.%) catalyst. This shows that phosphorus plays some role to favor the enrichment of the catalyst surface with Co sites. In the case of the Co–P–B catalyst, the concentration of the surface Co sites is between that of Co–P and Co–B, being about 69 at.%. This result reveals that the role of P in the Co–P–B catalyst is to favor the enrichment of the surface with Co active sites. Li et al. [21] also observed higher Co concentration on the surface of Co–P and Co–P–B as compared to Co–B catalyst. Lee et al. [22] reported the same results using Ni-based amorphous alloy (Ni–P–B, Ni–P, and Ni–B). On the basis of the above results, we may conclude that the higher catalytic activity of the Co–P–B powder, as compared to Co–B and Co–P, may be attributed to the synergistic effects occurring from the alloying P and B in which the former element is able to create high number of Co active sites on the surface, while the later element provides the necessary electron density to Co active sites for the catalytic activity.

3.3. Role of metalloids (P and B)

After these preliminary studies, Co–P–B amorphous alloys were synthesized with different B/P molar ratio in order to further investigate the effect of B and P concentration on catalytic activity. The hydrogen generation yield was measured as a function of time (Fig. 4) by hydrolysis of alkaline $NaBH_4$ (0.025 M) solution using different B/P molar ratio in Co–P–B catalyst powders. The inset of Fig. 4 shows the value of R_{max} obtained with Co–P–B catalyst having different B/P molar ratio. It is clearly evident that Co–P–B powder shows higher R_{max} than the Co–B independent of B/P molar ratio used: this further proves that the inclusion of P creates more Co active sites on the surface while B provides them with the required electron density. Initially R_{max} increases with the B/P ratio, to reach the maximum when B/P molar ratio is equivalent to 2.5, and then decreases further. At high B/P molar ratio the concentration of P is unable to provide enough active Co sites on the surface, while at low B/P molar ratio the concentration of B is insufficient to fulfill the requirment of electron density to all the excess Co active site on the surface. The above considerations help to explain the trend of the results in the inset of Fig. 4, although the maximum H_2 generation rate obtained at the B/P molar ratio of 2.5 is not clearly understood. Basic calculations of atomic site occupation as well as of electron transfer are necessary to further understand the mechanism, which is outside the scope of the present study. Here we would like to remark that the Co–P–B catalyst powders, for any B/P molar ratio, exhibit similar particle like morphology with average

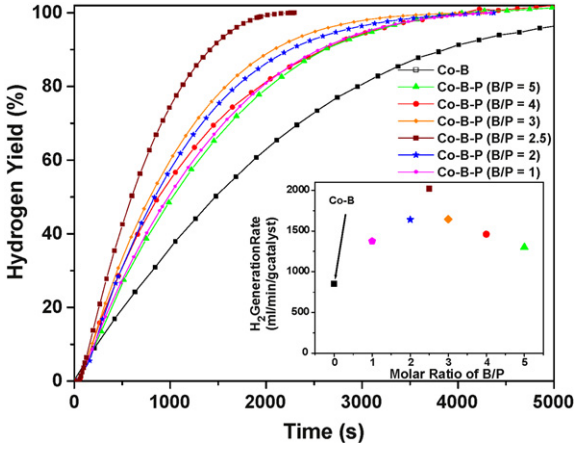

Fig. 4. Hydrogen generation yield as a function of reaction time obtained by hydrolysis of alkaline $NaBH_4$ (0.025 M) solution with Co–B and Co–P–B catalysts with different B/P molar ratio ranging from 1 to 5. Inset shows the maximum H_2 generation rate (R_{max}) obtained with Co–P–B catalyst as a function of B/P molar ratio. (For interpretation of the references to color in this artwork, the reader is referred to the web version of the article.)

size of 30–40 nm (figure not shown). Co–P–B catalyst with B/P molar ratio of 2.5 is used hereafter for the hydrolysis reaction.

3.4. Effect of heat-treatment

To study the effect of structural modification on catalytic activity, Co–P–B powder (with molar ratio B/P = 2.5) was heat-treated in Ar atmosphere at different temperatures upto 773 K for 2 hrs. The hydrogen generation yield, as a function of time, obtained by hydrolysis of alkaline $NaBH_4$ (0.025 M) solution using these heat-treated Co–P–B powders (15 mg) are reported in Fig. 5. There was no change in the catalytic activity of the Co–P–B powder after heat treatment at 673 K (R_{max} = ~2010 ml min^{-1} g^{-1}) and below 673 K (not shown in the Fig. 5) as compared to the untreated powder (R_{max} = ~2020 ml min^{-1} g^{-1}). On the contrary, the heat-treated sample at 773 K shows a decrease in the H_2 generation rate (R_{max} = 1250 ml min^{-1} g^{-1}) but, in any case, it is able to reach the 100% H_2 yield. This decrease in the catalytic activity might be due to the structural variation or particle agglomeration caused by heat treatment at 773 K. XRD pattern (Fig. 6) of the catalyst powder shows amorphous nature for both untreated Co–P–B powder and heat-treated sample at 673 K in Ar atmosphere. However, heat-treatment at 773 K in Ar atmosphere for 2 h causes partial crystallization of the powder as indicated by the presence of weak reflections of Co peaks in the XRD pattern. Thus after heat treatment at 773 K the amorphous Co–P–B powder starts to partially decompose into crystalline Co metal phase. SEM images (Fig. 7) clearly show the same surface morphology (particle nature) for the untreated Co–P–B powder and heat-treated sample at 673 K in Ar atmosphere. Co–P–B powder annealed below 673 K shows similar structure and morphology as that of untreated powder and heat treated at 673 K (figure not shown). However a few Co crystallites, as confirmed by EDS, surrounded by powder particles are clearly observed in the heated-treated sample at 773 K. In our previous work we have demonstrated that pure Co film was unable to show any catalytic activity for the hydrolysis of $NaBH_4$, while for the same reaction Co–B film showed excellent activity [16]. Thus it was proved that Co metal can exhibit catalytic activity only when alloyed with metalloid atoms such as B: this suggests that the low catalytic activity after the heat-treatment of Co–P–B powder at 773 K may be attributed to the formation of small amount of surface Co crystallites.

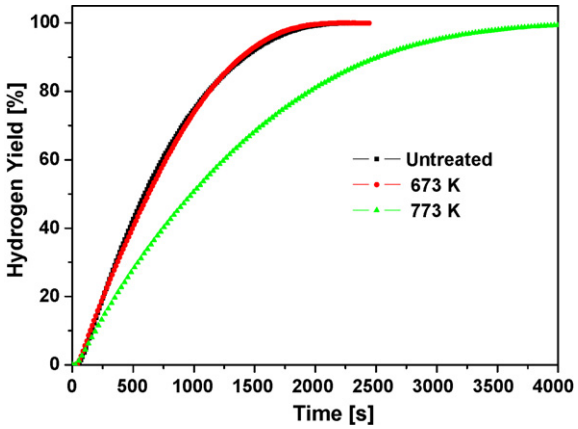

Fig. 5. Hydrogen generation yield as a function of reaction time obtained by hydrolysis of alkaline $NaBH_4$ (0.025 M) solution with Co–P–B (B/P = 2.5) catalyst powders untreated and heat-treated in Ar atmosphere at 673 and 773 K for 2 h. (For interpretation of the references to color in this artwork, the reader is referred to the web version of the article.)

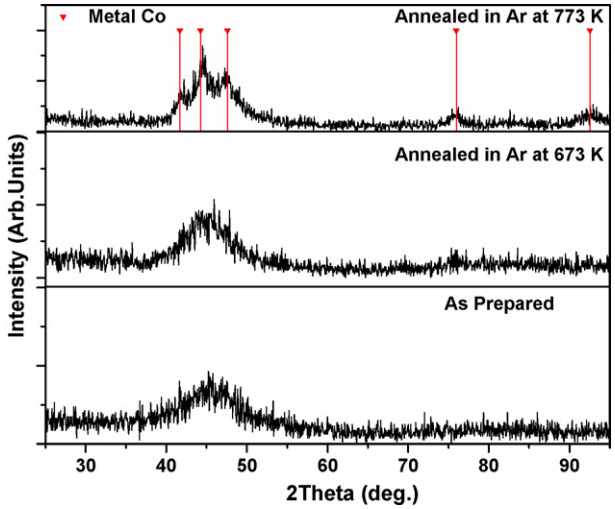

Fig. 6. XRD pattern of Co–P–B (B/P molar ratio = 2.5) catalyst powder untreated and heat-treated in Ar atmosphere at 673 and 773 K for 2 h.

3.5. Kinetics studies

Kinetic studies of the hydrolysis reaction are now required because they provide the necessary information concerning the role of the reactants and the catalyst behavior, which are important to develop a protocol for the design of a possible on board reactor. For any chemical reaction, the rate equation (r) is given by the power law [24] which is written as:

$$r = A\ \exp(-E/RT)\,[\text{reactants}]^{\alpha} \quad (1)$$

where A is pre-exponential factor, E is activation energy, R is universal gas constant, T is temperature, and α is the order of reaction.

During the catalytic hydrolysis of alkaline $NaBH_4$ solution, the hydrogen generation rate depends on many factors such as temperature, concentration of catalyst, $NaBH_4$ and NaOH. Thus the above Eq. (1) for the hydrogen generation rate (r) (ml min^{-1}), considering the factors involved in the hydrolysis of $NaBH_4$, is written as

$$r = A\ \exp(-E/RT)[\text{catalyst}]^{x}\,[NaBH_4]^{y}\,[NaOH]^{z} \quad (2)$$

Here, x, y, and z are the reaction orders with respect to concentration of catalyst, $NaBH_4$, and NaOH respectively. Several sets of experiments for catalytic hydrolysis of $NaBH_4$ were performed to

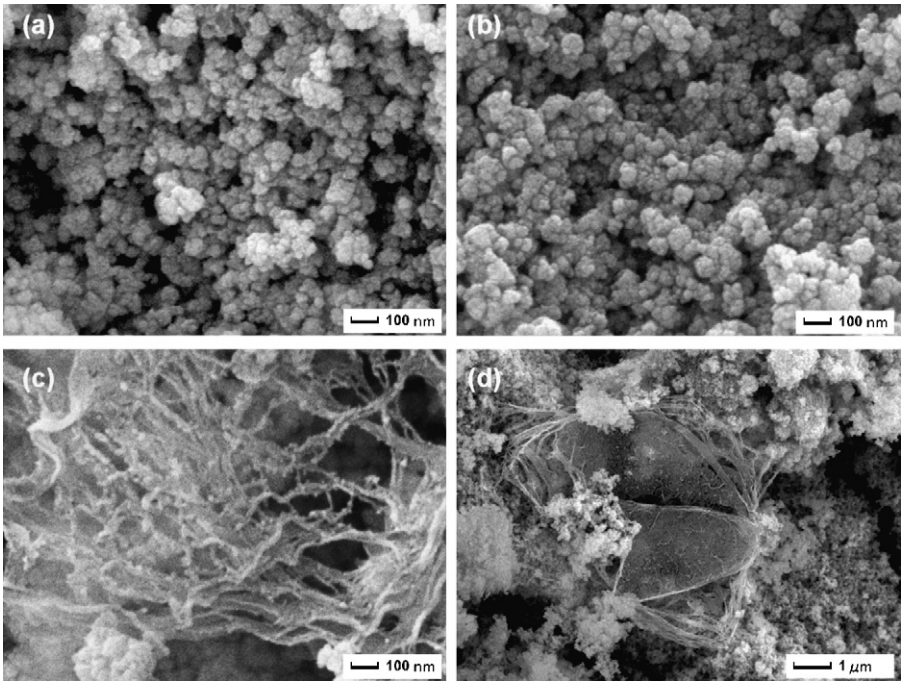

Fig. 7. SEM micrographs of: (a) untreated Co–P–B (B/P molar ratio = 2.5) catalyst powder and heat-treated (b) at 673 K, (c) and (d) at 773 K in Ar atmosphere for 2 h.

obtain the activation energy and the order of reaction for all the reactants.

3.5.1. Effect of solution temperature

Fig. 8 presents the H_2 generation yield as a function of time at different solution temperatures using alkaline $NaBH_4$ (0.025 M) solution and 15 mg of Co–P–B catalyst powder. As expected, H_2 generation rate increases with the temperature. Arrhenius plot of the hydrogen production rate using Co–P–B catalyst (inset of Fig. 8) gives the activation energy of about 32 ± 1 kJ mol^{-1}, within the experimental errors. This value is lower than the activation energy found by Amendola (47 kJ mol^{-1}) [10] using Ru catalyst. Kaufman and Sen [38], using different bulk metal catalysts, obtained 75 kJ mol^{-1} for cobalt, 71 kJ mol^{-1} for nickel, and 63 kJ mol^{-1} for Raney nickel. The value in the present case is comparable to that obtained with nano-particle assembled Co–B thin film (30 kJ mol^{-1}) [17], Pd/C powder (28 kJ mol^{-1}) [39], Co supported on α-Al_2O_3 (33 kJ mol^{-1}) [40], Ru nanoclusters (29 kJ mol^{-1}) [11] and Ru–C (37 kJ mol^{-1}) [41]. The favorable activation energy value obtained in the present work is again an evidence of the synergetic effects of P and B in Co–P–B to enhance the catalytic reaction.

3.5.2. Effect of catalyst concentration

In order to identify the reaction order with respect to the catalyst concentration, the hydrogen generation yield was measured by hydrolysis of alkaline $NaBH_4$ (0.025 M) solution at 298 K by using 5 different amounts of Co–P–B (B/P = 2.5) catalyst, namely 10, 15, 20, 25, and 30 mg (Fig. 9). As expected, as the amount of catalyst increases, the reaction takes much less time to reach the estimated hydrogen generation yield. In particular, when the temperature and the concentrations of all the other reactants are kept constant, then:

$$r \propto [\text{concentration of catalyst}]^x \quad (3)$$

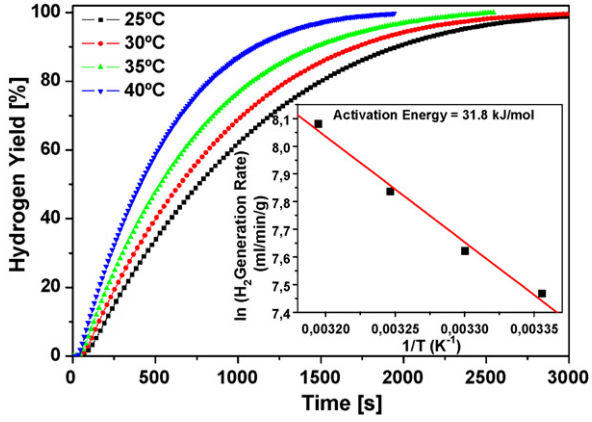

Fig. 8. Hydrogen generation yield as a function of reaction time with Co–P–B (B/P molar ratio = 2.5) catalyst measured at 4 different solution temperatures by hydrolysis of alkaline $NaBH_4$ (0.025 M) solution. Inset shows the Arrhenius plot of the H_2 generation rates with Co–P–B (B/P molar ratio = 2.5) powder. (For interpretation of the references to color in this artwork, the reader is referred to the web version of the article.)

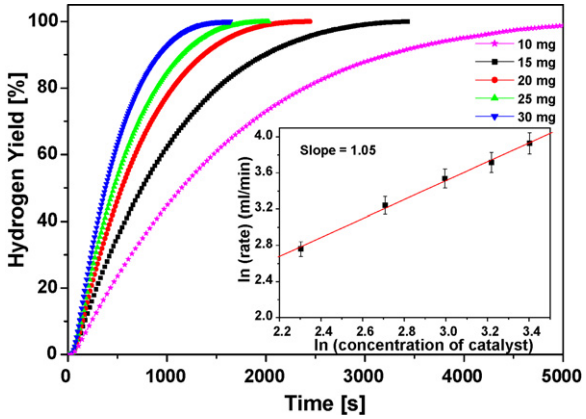

Fig. 9. Hydrogen generation yield as a function of reaction time with Co–P–B (B/P molar ratio = 2.5) catalyst of 5 different concentrations obtained by hydrolysis of alkaline $NaBH_4$ (0.025 M) solution. Insert shows the plot of ln(H_2 generation rate) vs ln(concentration of catalyst). (For interpretation of the references to color in this artwork, the reader is referred to the web version of the article.)

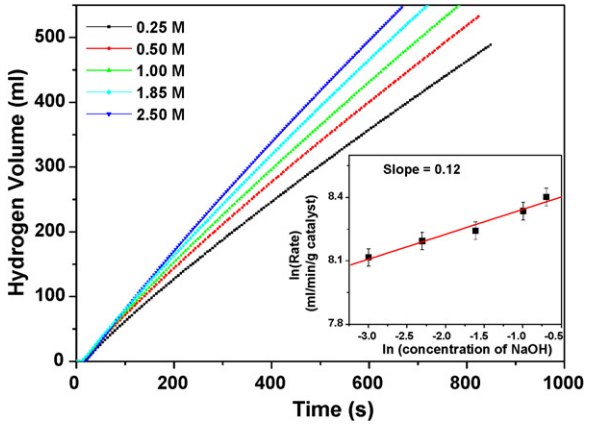

Fig. 10. Hydrogen generated volume as a function of reaction time with Co–P–B (B/P molar ratio = 2.5) catalyst obtained by hydrolysis of alkaline $NaBH_4$ (0.25 M) solution containing 5 different concentrations of NaOH ranging from 0.25 to 2.5 M. Insert shows the plot of ln(H_2 generation rate) vs ln(concentration of NaOH) to determine the reaction order with respect to NaOH. (For interpretation of the references to color in this artwork, the reader is referred to the web version of the article.)

The plot of ln(r) vs ln(concentration of catalyst) permits to obtain a straight line as seen in the inset of Fig. 9 and the slope of the straight line provides the value of order of reaction (x) with respect to the concentration of the catalyst. The value of the slope is evaluated to be 1.05 ± 0.02 within the experimental errors thus indicating that the hydrolysis of $NaBH_4$ is a first order reaction with respect to the concentration of Co–P–B powder catalyst. First-order kinetic was also obtained with respect to Pd concentration in Pd–C catalyst powder as reported in our previous work [8] while investigating the kinetics of $NaBH_4$ hydrolysis using ^{11}B NMR measurements. Ozkar et al. [11] and Demirci et al. [25] also showed first order kinetics for Ru catalyst during the hydrolysis of $NaBH_4$.

3.5.3. Effect of NaOH concentration

The hydrolysis reaction with $NaBH_4$ in water, without any catalyst, is suppressed by controlling the pH of the reaction solution; therefore it is important to investigate the effect of NaOH concentration on the hydrolysis reaction. This was carried out by measuring the volume of the generated H_2 from hydrolysis of alkaline $NaBH_4$ by using 5 different NaOH concentrations, namely: 0.25, 0.50, 1, 1.85, and 2.5 M in the starting solution. The concentration of $NaBH_4$ and Co–P–B catalyst were kept constant at 0.25 M and 15 mg respectively, during the hydrolysis reaction. The results are reported in Fig. 10. When the NaOH content is increased from 0.25 to 2.5 M, it shows a positive effect on the hydrogen generation rate (R_{max}). In the inset of the Fig. 10 we show the plot of ln(rate) vs ln(concentration of NaOH) which is fitted linearly with the positive slope of 0.12, the reaction order for NaOH. The effect of NaOH concentration on the hydrolysis of $NaBH_4$ greatly depends on the type of catalyst used for reaction. Few investigations on Co and Ni based catalysts [42,43] showed the increase in hydrogen generation rate with the increase in NaOH concentration. Zhang et al. [24], by using Ni-supported catalyst reported a value of 0.13, similar to ours, for the reaction order with respect to NaOH concentration. The authors suggested that the desorption of $B(OH)_4^-$ from the catalyst surface is influenced by the NaOH concentration which provides the renewal of the active site involved in the reaction (see also [8]). However, reports on Ru-based catalyst [41,42] showed a large negative effect with respect to NaOH concentration and authors explained this effect on the basis of reduction in water activity. However, for our Co–P–B catalyst the increase of NaOH concentration is beneficial for the hydrogen reactor because the addition of NaOH in the $NaBH_4$ solution not only increases the R_{max} but also keeps the $NaBH_4$ stable for a longer period of time.

3.5.4. Effect of $NaBH_4$ concentration

There is a lot of variation in literature of the reported value of reaction order for the hydrolysis of $NaBH_4$ with respect to the concentration of $NaBH_4$. A few number of researchers reported a zero order kinetics meaning that the hydrolysis does not depend on the $NaBH_4$ concentration [3,11,44,45]. Non-zero order kinetics was demonstrated by small group of researchers [8,40,41,46,47] including authors reporting negative order [24,40,46] or first order [8,11,47] kinetics with respect to $NaBH_4$ concentration. To resolve the above issue and gain better understanding, a wide range of $NaBH_4$ molar concentrations (0.005, 0.015, 0.025, 0.035, 0.050, 0.075, 0.1, 0.15, and 0.25 M) were used in the present study, for the catalytic hydrolysis reaction of $NaBH_4$. In the present work, the concentrations of NaOH and of catalyst were kept constant at 0.1 M and 15 mg respectively.

The catalytic activity data were grouped into two sets: in the first set, low concentrations of $NaBH_4$ (0.005, 0.015, 0.025, 0.035, 0.050 M) were considered and hydrogen generated volume as a function of time was plotted (see Fig. 11a). It can be seen that as the concentration of $NaBH_4$ increases from 0.005 to 0.05 M the hydrogen generation rate increases. In Fig. 11b we have plotted the ln(rate) vs ln(concentration of $NaBH_4$) and the data points are fitted linearly with a slope of 0.95 indicating the first order kinetics. In

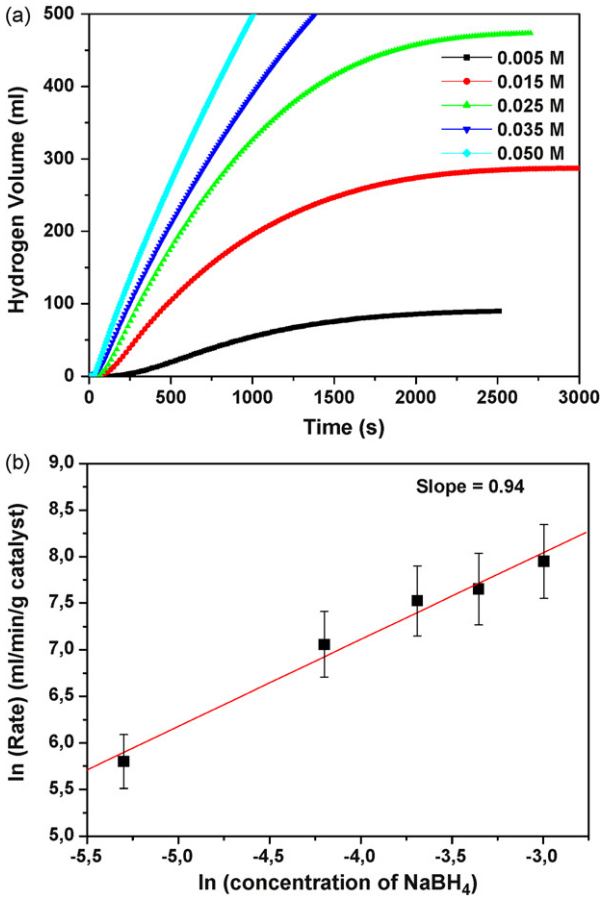

Fig. 11. (a) Hydrogen generated volume as a function of reaction time with Co–P–B (B/P molar ratio = 2.5) catalyst obtained by hydrolysis of alkaline $NaBH_4$ solution containing different concentrations of $NaBH_4$ ranging from 0.005 to 0.05 M. (b) Plot of ln(H_2 generation rate) vs ln(concentration of $NaBH_4$) to determine the reaction order with respect to $NaBH_4$. (For interpretation of the references to color in this artwork, the reader is referred to the web version of the article.)

the second set, the hydrogen generated volume was determined for higher concentrations of $NaBH_4$ (0.075, 0.1, 0.15, and 0.25 M) (see Fig. 12). In this case no change in the hydrogen generation rate with the increase in $NaBH_4$ concentration is observed. Inset of Fig. 12 shows the ln(rate) vs ln(concentration of $NaBH_4$) graph with slope of 0.07 after linear fitting: near-zero value of the slope indicates the zero order kinetics with respect to the $NaBH_4$ concentration. The above results clearly show that the order of reaction with respect to $NaBH_4$ concentration depends on the amount of $NaBH_4$ used in the starting solution. It changes from 1 to 0 value as the concentration is increased. Guella et al. [8] (for Pd supported on carbon), Shang et al. [41] (for Ru supported on carbon), and Pena-Alonso et al. [47] (for PdPt-carbon nanotubes) showed the first order kinetics for the $NaBH_4$ concentration, with starting solution containing low concentration of $NaBH_4$. The zero order kinetics for the $NaBH_4$ concentration proposed by Amendola et al. [3] (for Ru catalyst), Kojima et al. [44] (for Pt–$LiCoO_2$), and Ozkar et al. [11] (for Ru nanoclusters) was reported for higher concentration of $NaBH_4$. To gain better insight, let us investigate on this point further.

The $NaBH_4$ concentration decreases with time as the hydrogen is produced during the hydrolysis reaction: this fact can be used to estimate the reaction order with respect to $NaBH_4$ as the amounts of the catalyst and NaOH remain constant during the reaction. In zero order reaction, the H_2 production volume as a function of time has a linear dependence,

$$\frac{d[H_2]}{dt} = 4k_0. \quad (4)$$

where k_0 is the rate constant of the zero order reaction.

In the first order reaction, the H_2 production volume as a function of time has an exponential dependence as described by

$$[H_2](t) = [H_2]_{max}(1 - e^{-k_1 t}) = 4[[BH_4^-]_0(1 - e^{-k_1 t})], \quad (5)$$

where $[BH_4^-]_0$ is the initial molar concentration of sodium borohydride in the solution and k_1 is the overall rate constant of the first order reaction. Experimental data of H_2 production volume as a function of time can be fitted using Eqs. (4) or (5) by keeping the reaction order and the rate constant as variables. The best fitted curves give the values of the reaction order and the rate constant. Fig. 13 reports the hydrogen volume produced as function of time by hydrolysis of low (0.025 M) and high (0.25 M) concentration of $NaBH_4$. The plot corresponding to 0.025 M $NaBH_4$ could be fitted with only Eq. (5) which indicates the first order kinetics with respect to $NaBH_4$ concentration. A linear fit is achieved for the hydrogen volume plot corresponding to 0.25 M of $NaBH_4$ in the starting solution, describing zero order kinetics. The results obtained by this fitting method also confirm our previous observation that the hydrolysis reaction order with respect to the $NaBH_4$ depends on the amount of $NaBH_4$ used in the starting solution.

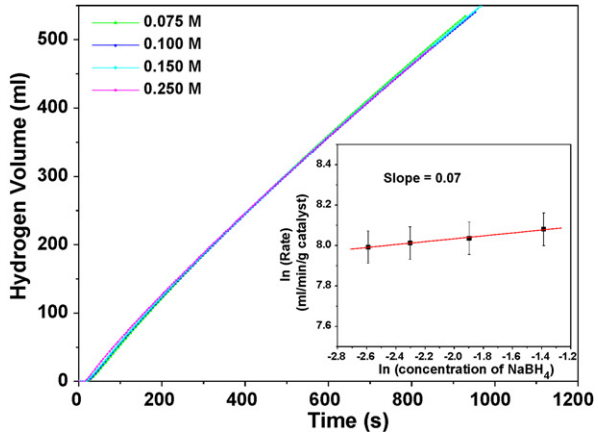

Fig. 12. Hydrogen generated volume as a function of reaction time with Co–P–B (B/P molar ratio = 2.5) catalyst obtained by hydrolysis of alkaline $NaBH_4$ solution containing different concentrations of $NaBH_4$ ranging from 0.075 to 0.25 M. Inset shows the plot of ln(H_2 generation rate) vs ln(concentration of $NaBH_4$) to determine the reaction order with respect to $NaBH_4$. (For interpretation of the references to color in this artwork, the reader is referred to the web version of the article.)

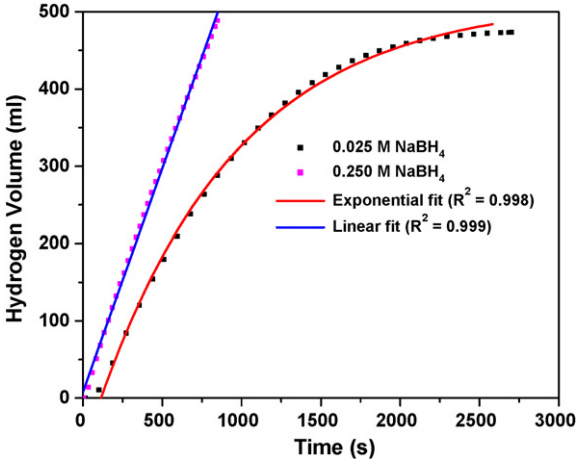

Fig. 13. Hydrogen generated volume as a function of reaction time with Co–P–B (B/P molar ratio = 2.5) catalyst obtained by hydrolysis of alkaline $NaBH_4$ solution containing low (0.025 M) and high (0.25 M) concentrations of $NaBH_4$. Symbols represent the experimental value and the solid line is obtained by fitting. (For interpretation of the references to color in this artwork, the reader is referred to the web version of the article.)

To understand the above results, we consider two simple steps involved in the catalytic hydrolysis reaction of $NaBH_4$ on the surface of the metal catalyst [45]: (1) absorption of BH_4^- on the surface active sites of the catalyst, and (2) reaction of this absorbed species to generate H_2. At low concentration of $NaBH_4$, the hydride/catalyst molar ratio is low which means that the catalyst surface is not completely covered with BH_4^- reactants and there are some unsaturated active sites on the surface available for the reaction. Thus, the first order kinetics involving diffusion of BH_4^- on the catalyst surface is the rate limiting step. At high hydride/catalyst molar ratio, the zero order kinetics is due to the BH_4^- induced dynamic saturation of the active sites on the catalyst surface during the reaction.

For practical application such as on-board hydrogen generation method for portable PEM fuel cells, high concentration of $NaBH_4$ is necessary, and thus the rate equation for the hydrolysis of alkaline $NaBH_4$ using Co–P–B catalyst is given by:

$$r = A \exp(-32000/RT)[\text{Co–P–B catalyst}]^{1.05}[NaBH_4]^{0.07}[NaOH]^{0.12} \quad (6)$$

3.6. Stability of catalyst

In a recent review article, Wee et al. [48] reported that one of the major difficulties for the development of the Borohydride-PEMFC is the catalyst tolerance to deactivation. In application field, the catalyst generally remains exposed to the ambient atmosphere and deactivation may intervene because of the oxide formation. To investigate the effect of ambient atmosphere on our newly developed catalysts, we prepared Co–P–B powder and exposed it to the ambient condition. The catalyst powder was then used a few times at an interval of 10–12 days for catalytic hydrolysis of alkaline $NaBH_4$ solution (0.025 M) (Fig. 14). The exposure of Co–P–B catalyst to the ambient condition for 10 days causes a little delay time to start the catalytic reaction, with a small decrease in the reaction rate, as compared to the fresh powder. However, after this initial efficiency failure, H_2 generation rate increases rapidly and

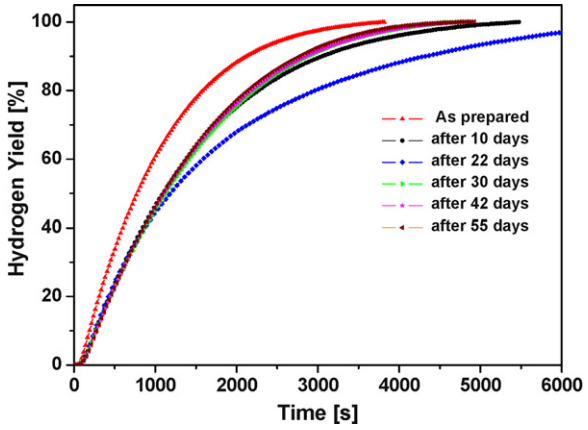

Fig. 14. Hydrogen generation yield as a function of reaction time obtained by hydrolysis of alkaline $NaBH_4$ (0.025 M) solution with Co–P–B (B/P molar ratio = 2.5) catalyst exposed to ambient atmosphere for several intervals of time. (For interpretation of the references to color in this artwork, the reader is referred to the web version of the article.)

the expected hydrogen yield is produced. This initial reduction in efficiency might be due to the formation of an oxide layer on the surface of the catalyst during exposure to the ambient atmosphere [22]. However, the reaction activity rapidly increases when the degraded sites get reactivated for the reasons unknown to us at present. Further exposure of the catalyst does not cause much change in R_{max} and each time 100% hydrogen yield is obtained (see Fig. 14). This study shows that our catalyst is quite stable against deactivation due to ambient atmosphere.

3.7. Durability of catalyst

Reusability and durability of the catalyst are other important factors to be considered before moving towards applications. A specific experiment was performed to recycle the sample many times as described in the following steps: (1) hydrolysis reaction course, (2) recollection of the powder, (3) washing with distilled water and ethanol before drying at around 323 K under continuous N_2 flow. Hydrogen generation yield as a function of time, for a number of runs, is reported in Fig. 15. It is clearly observed that after every run the R_{max} decreases, but each time the catalyst is able to produce 100% hydrogen yield. The small decrease in efficiency may be due to partial inactivation caused on the surface of the catalyst by the $NaBO_2$ formation during the reaction. Focused studies are under

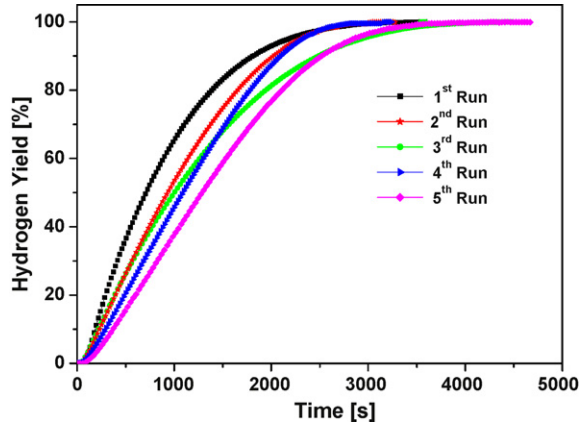

Fig. 15. Cyclic behavior of Co–P–B (B/P molar ratio = 2.5) catalyst powder on hydrogen generation yield as a function of reaction time measured using hydrolysis of 0.025 M $NaBH_4$ alkaline solution. (For interpretation of the references to color in this artwork, the reader is referred to the web version of the article.)

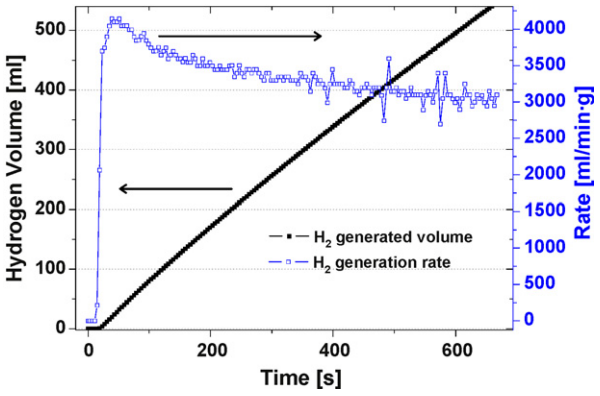

Fig. 16. Hydrogen generated volume and rate as a function of reaction time with Co–P–B (B/P molar ratio = 2.5) catalyst obtained by hydrolysis of alkaline $NaBH_4$ solution containing 1 wt% of $NaBH_4$ and 5 wt% of NaOH.

Table 2
Comparison of maximum H_2 generation rate between our present Co–P–B catalyst powder and various catalysts reported in the literature.

Catalyst type	$NaBH_4$ concentration	Max. H_2 generation rate, R_{max} (ml min^{-1} g^{-1} catalyst)	Ref.
Ru on IRA	10 wt%	~480	[10]
Ni_xB	1.5 wt%	~233	[42]
Pt–$LiCoO_2$	20 wt%	~3,100	[49]
PtRu–$LiCoO_2$	5 wt%	~2,400	[9]
Pt/C	10 wt%	~23,000	[7]
Co–B powder	5 wt%	~1,500	[44]
Co–B film	1 wt%	~3,300	[16]
Ni–Co–B powder	3 wt%	~2,600	[50]
Co/γ–Al_2O_3	5 wt%	~220	[40]
Electrodeposited Co-P	10 wt%	954	[51]
Our Co–P–B powder	1 wt%	~4,150	–

way to investigate the catalyst surface after the reaction in order to improve the catalyst durability.

In order to compare the efficiency of our Co–P–B catalyst to that of catalysts reported in the literature, a hydrogen generation measurement by hydrolysis reaction was performed using 1 wt% of $NaBH_4$ and 5 wt% of NaOH with 15 mg of catalyst (see Fig. 16). R_{max} of about ~4150 ml min^{-1} g^{-1} is obtained which is far better than many other catalysts and comparable to the noble metal like Ru (see Table 2 for comparison). Only carbon supported Pt (Pt/C) shows higher H_2 generation rate (23,000 ml min^{-1} g^{-1}) than our catalyst powder [7]. However, Pt is one of the costliest materials and not preferable for commercial use. R_{max} of about 4000 ml min^{-1} g^{-1} obtained with our Co–P–B powder can generate 720 W for Proton Exchange Membrane Fuel Cells (0.7 V) which is necessary for portable devices.

4. Conclusions

A careful analysis was performed on catalytic hydrolysis of $NaBH_4$ by using amorphous catalyst alloy powders: Co–P, Co–B, and Co–P–B. Superior efficiency of Co–P–B amorphous powder catalyst for hydrogen production, as compared to that of Co–B and Co–P, was observed and further investigated. The roles of the metalloids (B and P) in the Co–P–B catalyst were investigated by regulating the B/P molar ratio in the starting material. The enhanced activity obtained with Co–P–B (B/P molar ratio = 2.5) powder catalyst was mainly attributed to synergic effects caused by P and B atoms in the catalyst: the former element creates high number of Co active sites on the surface, while the later element provides the necessary electron density to Co active sites for the catalytic activity. The resulting effective activation energy for hydrolysis of $NaBH_4$ with

Co–P–B catalyst (B/P molar ratio = 2.5) is quite low (32 kJ mol^{-1}) as compared to the literature data for other catalysts. In addition, the kinetic studies on hydrolysis reaction of $NaBH_4$ with Co–P–B catalyst disclose that the concentrations of both NaOH and the catalyst influence the hydrogen generation rate. The zero order reaction kinetics is observed with respect to $NaBH_4$ concentration with high hydride/catalyst molar ratio while the first order reaction kinetics is observed at low hydride/catalyst molar ratio. At high hydride/catalyst molar ratio, the zero order kinetics is due to the BH_4^- induced dynamic saturation of the active sites on the catalyst surface during the reaction. While in the case of low hydride/catalyst molar ratio, the catalyst surface is not completely covered with BH_4^- reactants and there are few unsaturated active sites on the surface which are available for the reaction. Thus, the first order kinetics is related to the diffusion of BH_4^- on the catalyst surface.

Stability, reusability, and durability of Co–P–B catalyst were investigated and found relevant for applications such as on-board hydrogen generation method for portable PEM fuel cells. It was found that by using B/P molar ratio of 2.5 in Co–P–B catalyst, highest H_2 generation rate of about ~4000 ml min^{-1} g^{-1}, can be achieved. This can generate 720 W for Proton Exchange Membrane Fuel Cells (0.7 V) which is necessary for portable devices.

Acknowledgements

We thank N. Bazzanella for SEM–EDS analysis, C. Armellini for XRD analysis, M. Filippi for XPS analysis, and Prof. D.C. Kothari for English revision of the paper. The research activity is financially supported by the Hydrogen-FISR Italian project.

References

[1] A.L. Dicks, J. Power Sources 61 (1996) 113.
[2] R.B. Biniwale, S. Rayalu, S. Devotta, M. Ichikawa, Int J. Hydrogen Energy 33 (2008) 360.
[3] S.C. Amendola, S.L. Sharp-Goldman, M.S. Janjua, M.T. Kelly, P.J. Petillo, M. Binder, J. Power Sources 85 (2000) 186.
[4] Z.P. Lin, N. Morigazaki, B.H. Liu, S. Suda, J. Alloys Compd. 349 (2003) 232.
[5] J. lee, K.Y. Kong, C.R. Jung, E. Cho, S.P. Yoon, J. Han, T.-G. Lee, S.W. Nam, Catal. Today 120 (2007) 305.
[6] H.I. Schlesinger, H.C. Brown, A.B. Finholt, J.R. Gilbreath, H.R. Hockstra, E.K. Hydo, J. Am. Chem. Soc. 85 (1963) 215.
[7] Y. Bai, C. Wu, F. Wu, B. Yi, Mater. Lett. 60 (2006) 2236.
[8] G. Guella, C. Zanchetta, B. Patton, A. Miotello, J. Phys. Chem. B 110 (2006) 17024.
[9] P. Krishnan, T.H. Yang, W.Y. Lee, C.S. Kim, J. Power Sources 143 (2005) 17.
[10] S.C. Amendola, S.L. Sharp-Goldman, M.S. Janjua, N.C. Spencer, M.T. Kelly, P.J. Petillo, M. Binder, Int. J. Hydrogen Energy 25 (2000) 969.
[11] S. Özkar, M. Zahmakiran, J. Alloys Compd. 404–406 (2005) 728.
[12] U.B. Demirci, F. Garin, Catal. Commun. 9 (2008) 1167.
[13] S. Suda, Y.M. Sun, B.H. Liu, Y. Zhou, S. Morimitsu, K. Arai, N. Tsukamoto, M. Uchida, Y. Candra, Z.P. Li, Appl. Phys. A: Mater. Sci. Process. 72 (2001) 209.
[14] B.H. Liu, Z.P. Li, S. Suda, J. Alloys Compd. 415 (2006) 288.
[15] S.U. Jeong, E.A. Cho, S.W. Nam, I.H. Oh, U.H. Jung, S.H. Kim, Int. J. Hydrogen Energy 32 (2007) 1749.
[16] N. Patel, G. Guella, A. Kale, A. Miotello, B. Patton, C. Zanchetta, L. Mirenghi, P. Rotolo, Appl. Catal. A: Gen. 323 (2007) 18.
[17] N. Patel, R. Fernandes, G. Guella, A. Kale, A. Miotello, B. Patton, C. Zanchetta, J. Phys. Chem. C 112 (2008) 6968.
[18] H. Li, Y. Wu, Y. Wan, J. Zhang, W. Dai, M. Qiao, Catal. Today 93 (2004) 493.
[19] X. Yua, H. Li, J.F. Deng, Appl. Catal. A: Gen. 199 (2000) 191.
[20] K.S. Eom, K.W. Cho, H.S. Kwon, J. Power Sources 180 (2008) 484.
[21] H. Li, P. Yang, D. Chu, H. Li, Appl. Catal. A: Gen. 325 (2007) 34.
[22] S.P. Lee, Y.W. Chen, J. Mol. Catal. A: Chem. 152 (2000) 213.
[23] M.M. Kreevoy, J.E.C. Hutchins, J Am. Chem. Soc. 94 (1972) 6371.
[24] Q. Zhang, Y. Wu, X. Sun, J. Ortega, Ind. Eng. Chem. Res. 46 (2007) 1120.
[25] U.B. Demirci, F. Garin, J. Mol. Catal. A: Chem. 279 (2008) 57.
[26] D.A. Lyttle, E.H. Jensen, W.A. Struck, Anal. Chem. 24 (1952) 1843.
[27] C. Zanchetta, B. Patton, G. Guella, A. Miotello, Meas. Sci. Technol. 18 (2007) N21.
[28] G.W. Pei, W.L. Zhong, S.B. Yue, Univ. Press. Jinan (1989) 453.
[29] A. Baiker, Faraday Discuss. Chem. Soc 87 (1989) 239.
[30] W.L. Dai, M.H. Qiao, J.F. Deng, Appl. Surf. Sci. 120 (1997) 119.
[31] A. Lebugle, U. Axelsson, R. Nyholm, N. Martensson, Phys. Scr. 23 (1981) 825.
[32] H. Li, H.X. Li, W.L. Dai, Z. Fang, J.F. Deng, Appl. Surf. Sci. 152 (1999) 25.
[33] H. Li, Q. Zhao, H. Li, J. Mol. Catal. A: Chem 285 (2008) 29.
[34] H. Li, W. Wang, H. Li, J.F. Deng, J. Catal. 194 (2000) 211.
[35] W.S. Xia, Y. Fan, Y.S. Jiang, Y. Chen, Appl. Surf. Sci. 103 (1996) l.
[36] H. Li, Y. Wu, H. Luo, M. Wang, Y. Xu, J. Catal. 214 (2003) 15.
[37] S. Yoshida, H. Yamashita, T. Funabiki, T. Yonezawa, J. Chem. Soc. Faraday Trans. 80 (1984) 1435.
[38] C.M. Kaufman, B. Sen, J. Chem. Soc. Dalton Trans. 2 (1985) 307.
[39] N. Patel, B. Patton, C. Zanchetta, R. Fernandes, G. Guella, A. Kale, A. Miotello, Int. J. Hydrogen Energy 33 (2008) 287.
[40] W. Ye, H. Zhang, D. Xu, L. Ma, B. Yi, J. Power Sources 164 (2007) 544.
[41] Y. Shang, R. Chen, Energy Fuels 20 (2006) 2149.
[42] D. Hua, Y. Hanxi, A. Xinping, C. Chuansin, Int. J. Hydrogen Energy 28 (2003 1095).
[43] S.U. Jeong, R.K. Kim, E.A. Cho, H.J. Kim, S.W. Nam, I.H. Oh, S.A. Hong, S.H. Kim, J. Power Sources 144 (2005) 129.
[44] Y. Kojima, K.I. Suzuki, Y. Kawai, J. Power Sources 155 (2006) 325.
[45] J.S. Zhang, W.N. Delgass, T.S. Fisher, J.P. Gore, J. Power Sources 164 (2007) 772.
[46] M. Mitov, R. Rashkov, N. Atanassov, J. Mater. Sci. 42 (2007) 3367.
[47] R. Pẽna-Alonso, A. Sicurelli, E. Callone, G. Carturan, R. Raj, J. Power Sources 165 (2007) 315.
[48] J.H. Wee, J. Power Sources 155 (2006) 329.
[49] Y. Kojima, K.I. Suzuki, K. Fukumoto, M. Sasaki, T. Yamamoto, Y. Kawai, H. Hayashi, Int. J. Hydrogen Energy 27 (2002) 1029.
[50] J.C. Ingersoll, N. Mani, J.C. Thenmozhiyal, A. Muthaian, J. Power Sources 173 (2007) 450.
[51] K.W. Cho, H.S. Kwon, Catal. Today 120 (2007) 298.